Journal of Magnetic Resonance 207 (2010) 242–250

Contents lists available at ScienceDirect

Journal of Magnetic Resonance

journal homepage: www.elsevier.com/locate/jmr

Z-spectroscopy with Alternating-Phase Irradiation

Johanna Närväinen [a,*], Penny L. Hubbard [b], Risto A. Kauppinen [c], Gareth A. Morris [b]

[a] A.I. Virtanen Institute for Molecular Sciences, University of Eastern Finland, Finland
[b] School of Chemistry, University of Manchester, Oxford Road, Manchester M13 9PL, United Kingdom
[c] Dartmouth Medical School, Hinman Box 7785, 706 Vail Building, Hanover, NH 03755, USA

ARTICLE INFO

Article history:
Received 14 July 2010
Revised 8 September 2010
Available online 15 September 2010

Keywords:
Z-spectroscopy
Magnetization transfer
Chemical exchange

ABSTRACT

Magnetization transfer (MT) MRI and Z-spectroscopy are tools to study both water–macromolecule interactions and pH-sensitive exchange dynamics between water and the protons of mobile chemical groups within these macromolecules. Both rely on saturation of frequencies offset from water and observation of the on-resonance water signal. In this work, an RF saturation method called Z-spectroscopy with Alternating-Phase Irradiation (ZAPI) is introduced. Based on the T_2-selectivity of the irradiation pulse, ZAPI can be used to separate the different contributions to a Z-spectrum, as well as to study the T_2 distribution of the macromolecules contributing to the MT signal. ZAPI can be run at resonance for water and with low power, thus minimizing problems with specific absorption rate (SAR) limits in clinical applications. In this paper, physical and practical aspects of ZAPI are discussed and the sequence is applied *in vitro* to sample systems and *in vivo* to rat head to demonstrate the method.

1. Introduction

The effects of off-resonance radiofrequency (RF) irradiation on the on-resonance magnetization in the NMR spectrum of a system in which magnetization is exchanging between different pools have been studied since the 1960s [1]. In 1990, Grad and Bryant studied exchange between cross-linked BSA and water by measuring the water magnetization as a function of the offset of a presaturating radiofrequency field, naming the experiment Z-spectroscopy [2].

A Z-spectrum records the z magnetization of water after some period of RF irradiation as a function of the frequency used, and typically contains three main components.

First, on resonance, virtually all of the water magnetization is lost as a result of direct saturation (DS) of free water by the presaturating irradiation. The width of this approximately Lorentzian-shaped direct saturation peak depends primarily on the relaxation times (T_1, T_2) of water and on the amplitude of the RF irradiation (B_1).

Second, in systems with short T_2, solid or semi-solid components such as the macromolecular components of tissue, exchange of magnetization between water and solid-like pools, causes a broad decrease in signal over a range of tens of kHz. The shape of this feature is determined by the structure and rigidity of the macromolecular pool and by the relaxation properties of the spin pools involved, as well as by the experimental parameters used.

Third, any exchange of magnetization that occurs on a suitable timescale between water and other long T_2 components creates sharp dips in water signal at the chemical shifts of those components, typically a few ppm from the water resonance.

For historical reasons, the second type of feature is generally referred to as magnetization transfer (MT); this is the main source of contrast in magnetization transfer contrast (MTC) imaging. We use here the complementary term magnetization exchange (ME) for the third type, to denote exchange between water and long T_2 components. Although a topic of frequent debate, the general consensus at present is that both cross-relaxation [3–5] and chemical exchange [6–10] contribute to the MT, but that the small ME dips observed in Z-spectra around 8.3 ppm *in vivo* [11] are a result of the pH-dependent chemical exchange of water with amide protons, found approximately 3.5 ppm downfield of the water resonance, and that cross-relaxation does not contribute significantly to this ME feature. As will be seen later, it is, however, likely that cross-relaxation is implicated in some other ME features.

Several mathematical models for MTC have been proposed [12–14], and the accuracy and stability of the solutions under different experimental conditions have been compared [15]. When a saturation pulse is delivered far (several tens of kHz) from water resonance, only resonances with very short T_2s are significantly affected, so the Z-spectrum in this region is dominated by MT. The MT envelope for biological tissues is slightly asymmetric about the water resonance [16], in part because the weighted average chemical shift of tissue is typically slightly less than that of water;

* Corresponding author. Address: University of Eastern Finland, P.O.B. 1627, 70211 KUOPIO, Finland. Fax: +358 17 163030.
E-mail address: johanna.narvainen@uef.fi (J. Närväinen).

1090-7807/$ - see front matter © 2010 Elsevier Inc. All rights reserved.
doi:10.1016/j.jmr.2010.09.004

it is best described by a Gaussian lineshape where there is a solid-like matrix, and by a super-Lorentzian in soft tissues with partial ordering [17]. Ideally, it would be desirable to measure MTC on resonance, where the influence of any difference in lineshape is at a minimum and the effect itself is at its maximum. Unfortunately, when using conventional methods for measuring MTC, the closer to resonance the irradiating field is applied, the stronger the DS of the water. The effects of any long-T_2 magnetization pools will also interfere with the measurement.

In contrast to the MT component of a Z-spectrum, ME components represent more specific types of interaction and are seen where the RF saturation falls close to the resonance of a spin pool with a relatively long T_2 (ms to tens of ms), with a rate constant for exchange with water protons typically in the range 10–100 s^{-1} [18,19]. The amide peak around 3.5 ppm from water is of particular interest, as one of the factors determining the amide–water exchange rate is pH [11,20]. The amide proton transfer ratio (APTR) has shown the potential to become a method for measuring pH *in vivo*. It has been used as source of contrast in rat middle cerebral artery occlusion (MCAO) [11] and in differentiating between tumor and edema in humans with brain tumors [18]. APTR was also recently applied in human brain at 7 T [21]. In the methodology presently used [11] the water signal is placed at exact resonance and the APTR is calculated by taking the difference between corresponding points either side of the water resonance, to produce a spectral asymmetry plot.

The APTR method sets out to eliminate the dominant, but approximately symmetric, effects of MT and direct water saturation. However, the asymmetry curve has a sloping baseline under the APTR signal, caused by the inherent asymmetry in the MT bandshape. This can either be fitted as a varying baseline and subtracted [22], which requires sampling the Z-spectrum at multiple frequencies, or assumed constant, which may not be appropriate for different tissue types and physiological conditions. A further problem is that any error in the choice of the nominal water frequency, and any asymmetric lineshape contributions from B_0 homogeneity, will lead to strong DS features in the asymmetry plot. Such features can be minimized by careful adjustment of the nominal zero frequency, usually by acquiring additional points near the expected position of resonance and finding the exact offsets by fitting a polynomial or an inverse Lorentzian to the central area for every pixel. The data in the APTR region, and on the other side, are then interpolated at the frequencies of interest. Acquiring the central Z-spectrum in the same way as the APTR data is time-consuming, as the saturation times are long. Another approach is to determine the exact water resonance frequency in each voxel by acquiring a narrow Z-spectrum containing only the DS component, using short irradiation pulses with very low amplitudes [23]. This kind of WASSR reference spectrum can be run with shorter repetition times, in a few minutes on clinical MRI scanners. The water offset can also be estimated from a conventional B_0 map [21] but finding the exact resonance for each pixel is not trivial [23].

It would be helpful not to have to rely on the asymmetry of the Z-spectrum for determining the rate of amide proton exchange; even better would be to be able to separate out all the different contributions (DS, MT, ME) to the spectrum. The relative magnitudes of the components vary depending on the experimental conditions (saturation power, details of the saturation pulse, duration of irradiation) and the properties of the system (relaxation times, linewidths and frequencies of the resonances involved, rates of different exchange processes, concentrations of the proton pools involved), all of which can change under different physiological and pathological conditions. There are mathematical models [11] that can allow the different components of a Z-spectrum to be extracted, but they typically require a large number of assumptions or a good deal of prior knowledge about the system. This is especially problematic when studying abnormal physiology or tissue types, as many NMR parameters may change simultaneously. Blind or semi-physical fitting and subtraction of components is another possibility, but requires the acquisition of data over a broad frequency range; this is generally too time-consuming, especially in clinical applications.

The presence of multiple contributions to Z-spectra thus both complicates the interpretation and to some extent restricts the application, of Z-spectroscopy. The degree of water saturation at a given pre-irradiation frequency can depend on two or more different mechanisms, so experimental methods that offer some discrimination between the different possibilities would potentially be very valuable. In this paper we investigate the possibility of discriminating experimentally between MT and other mechanisms, and introduce a method called Z-spectroscopy with Alternating-Phase Irradiation (ZAPI). This uses phase and/or amplitude modulation of a continuous pre-irradiation field to exploit the very different timescales of coherence loss between the MT and the DS and ME effects, allowing the selective saturation of short T_2 components. A fundamental distinction is drawn between incoherent response to irradiation, in which the rate of saturation is determined purely by the average of the square of the RF amplitude, and the more complex coherent response. In this work ZAPI was tested on egg white and tissue suspension phantoms at high Z-spectral resolution, and as a preparation block for MRI of rat head *in vivo*, and it is shown that the MT envelope can be measured without interference from direct saturation of water and other long-T_2 components. It is also shown that ZAPI provides a method for T_2-selective saturation, enabling studies of macromolecular T_2-distribution.

2. Theory

Any periodic modulated irradiation with period τ at a frequency ν_0 is equivalent to a set of continuous irradiations ("sidebands") of (complex) amplitudes a_i and frequencies $\nu_i = \nu_0 \pm n/\tau$ Hz, where n is zero or integer. In analyzing the effects of such irradiation on a net nuclear magnetization, while general analytical solutions of the Bloch equations exist [24–26], two useful special cases may be distinguished for which much simpler descriptions are available. The first may be termed the sideband approximation: where the period τ of the modulation is small compared both to the inverse of the RF amplitude and to T_2 ($\omega_1\tau \ll 1$, $\tau \ll T_2$) then the response of the spin system is coherent. Perturbation of the system is negligible far from sidebands, and close to a sideband is equal to that for a coherent radiation of amplitude a_i at the sideband frequency. Conversely, for a coherent radiofrequency field of maximum amplitude ω_1, if $\omega_1 T_2 \ll 1$, i.e. if the timescale of the irradiation is much slower than that of transverse relaxation (loss of coherence), the response to the irradiation is incoherent: the system is overdamped, and the approach to the steady state is exponential. This incoherent approximation typically applies to the macromolecular pool in Z-spectroscopy. Under these conditions the Bloch equations for the Cartesian magnetization components in a frame of reference rotating at the angular velocity ω of the radiofrequency irradiation

$$\frac{dM_x}{dt} = -R_2 M_x - \Delta M_y \tag{1a}$$

$$\frac{dM_y}{dt} = -R_2 M_y + \Delta M_x - \omega_1 M_z \tag{1b}$$

$$\frac{dM_z}{dt} = R_1(M_0 - M_z) + \omega_1 M_y \tag{1c}$$

reduce to

$$M_x = -\Delta M_y / R_2 \tag{2a}$$

$$M_y = -\omega_1 M_z R_2 / (R_2^2 + \Delta^2) \tag{2b}$$

$$\frac{dM_z}{dt} = R_1(M_0 - M_z) - \omega_1^2 R_2 M_z / (R_2^2 + \Delta^2) = R_1 M_0 - M_z \left[\frac{R_1(R_2^2 + \Delta^2) + \omega_1^2 R_2}{R_2^2 + \Delta^2} \right] \tag{2c}$$

where $R_1 = 1/T_1$, $R_2 = 1/T_2$, $\Delta = \gamma B_0 - \omega$ and $\omega_1 = -\gamma B_1$. T_1 is the longitudinal relaxation time, T_2 is the transverse relaxation time, γ is the magnetogyric ratio and M_0 is the equilibrium magnetization; B_0 and B_1 are the magnitudes of the static and RF fields, respectively.

In the incoherent approximation there is thus a simple monoexponential approach to the familiar steady-state solutions [29]. The rate constant for the approach of M_z to equilibrium is $R_1(M_0/M_z^{ss})$, where M_z^{ss} is the steady-state solution for M_z. The first part of Eq. (2c) shows that the rate is determined by two processes: spin–lattice relaxation, with rate constant R_1, and saturation, with rate constant $\omega_1^2 R_2/(R_2^2 + \Delta^2)$, or $\omega_1^2 T_2$ on resonance. The rate of saturation is proportional to the square of the RF amplitude, and to the quantity $R_2/(R_2^2 + \Delta^2)$, which is the natural lineshape of the spectrum, a Lorentzian of width $1/(\pi T_2)$ Hz. The observation that the rate of spectral transitions is proportional to the square of the perturbation multiplied by the spectrum is familiar from other forms of spectroscopy as Fermi's golden rule, and suggests that MT effects in solid and semi-solid systems should be describable by analogy, replacing the Lorentzian term in the saturation rate constant with the appropriate Gaussian or super-Lorentzian lineshape. One interesting corollary is that the shapes of Z-spectra are expected to show a dependence on irradiation time, with shorter irradiation times favouring central features.

The observation that the rate of saturation in the incoherent case ($\omega_1 T_2 << 1$) is determined by the square of the RF amplitude multiplied by T_2 has a number of useful consequences. First, it means that different spin pools may be probed by using different RF amplitudes. Thus the effects of high amplitude saturation are dominated by MT (large spin pools with short T_2), and the effects of low-amplitude saturation by ME (small spin pools with long T_2). *In vivo* the spin pools contributing to MT are much larger than the pools involved in ME, and significant MT is detected even with low-amplitude saturation. Second, it shows that, within the incoherent approximation, the amount of RF energy required to effect a given degree of saturation (and by extension, a given degree of MT contrast) increases rapidly away from resonance because of the decrease in rate of saturation. Third, again within the incoherent approximation, the degree of saturation achievable in a given time is determined by the average RF power deposition, *irrespective of the form of the irradiation*. Thus for a given average RF power, any modulation pattern that is slow on the timescale of decoherence for a given magnetization pool (T_2 for a Lorentzian bandshape, more generally of the order of the inverse of the linewidth) will give the same degree of saturation of that pool.

This is quite different from the coherent case ($\omega_1 T_2 >> 1$; low saturation amplitude, long T_2), where a change in modulation pattern can make the difference between negligible saturation and full saturation. The problem of discriminating between MT and ME/DS features in Z-spectroscopy can thus be addressed by seeking suitable modulation waveforms. The two cases examined here are square wave modulation (ZAPI), in which the phase of the RF is changed by 180° every $\tau/2s$, and sine wave (Z-spectroscopy with Alternating-Phase Irradiation and Sine Modulation, ZAPISM), where the amplitude of the RF waveform is given by $\omega_1 \sin(2\pi t/\tau)$. In both cases the DS effect of the irradiation on the water resonance (i.e. at ν_0) is small, because over a full cycle τ the water magnetization is simply rotated through a small angle away from equilibrium and then returned intact except for slight T_2 relaxation. Only at frequencies $\nu_0 \pm n/\tau$ (ZAPI) or $\nu_0 \pm 1/\tau$ (ZAPISM) is direct saturation effective, because the water magnetization rotates through an odd number of revolutions between phase changes of the RF and the effects of successive periods $\tau/2$ are cumulative [27]. The incoherent saturation of the macromolecular pool, however, which gives rise to MT, is unchanged except that the lower root mean square (rms) amplitude means that the RF power used for ZAPISM needs to be 3 dB higher for equal saturation. Comparing the results of constant-phase ($C\phi$) and alternating phase ($A\phi$, ZAPI or ZAPISM) experiments thus (a) allows the effects of MT and DS/ME to be distinguished, (b) allows MT to be measured at exact resonance without interference from DS, and (c) allows the contributions of magnetization pools with different T_2s to be probed by varying the modulation period τ. The ZAPISM method has the advantage that both sidebands fall well within the envelope of the macromolecular signal, and hence the SAR is kept to a minimum. In contrast, related methods using binomial pulses [28] or sequences of trains of rectangular pulses [29,30] have sideband patterns which extend much further and contribute much less efficiently to MT, increasing the SAR needed to achieve a given degree of saturation, and typically have sidebands much closer to resonance [31]. Compared to trains of binomials, ZAPISM offers improved discrimination due to the low B_1 used and the larger separation between sidebands. Similarly, ZAPISM requires much lower SAR than typical pulsed saturation patterns proposed for clinical use, such as Gaussian pulses lasting a few ms applied in bursts of several tens of pulses [32]. In those pulsed saturation experiments the steady state of the system is a result of periods of both irradiation and free precession, complicating the mathematical modelling and quantification of different processes. However, pulsed MT experiments enable shorter imaging times and can also be used to produce clear MT contrast at high field strengths [33]. Pulsed on-resonance techniques have also been used to study ME between water and exogenous lanthanide contrast agents resonating tens or hundreds of ppm from free water [30].

3. Experimental

3.1. NMR methods and samples

3.1.1. Spectroscopy

All spectroscopic data were acquired at 9.4 T on Varian INOVA 400 MHz spectrometers (Varian Inc., Walnut Creek, CA, USA). Z-spectra were measured at a range of RF amplitudes using a long low amplitude pre-irradiation RF pulse followed by a small crusher gradient and a detection pulse. In the ZAPI and ZAPISM sequences the RF phase was inverted every 100 μs (τ = 200 μs) so that on-resonance signals were saturated for $T_2 << \tau$ but unaffected for $T_2 >> \tau$. The repetition time was 33 s, irradiation time 20 s, and a low read pulse flip angle (~10°) was used in order to ensure approximately Lorentzian lineshapes irrespective of radiation damping [24].

Animal tissue samples were obtained from transcardially saline-perfused animals and homogenized with phosphate buffer (1 part tissue, 5 parts buffer). Experiments were performed on a Varian INOVA 400 spectrometer using saturation RF amplitudes ($\gamma B_1/2\pi$) of 33, 75, 150, and 300 Hz, for both coherent irradiation ($C\phi$) and the ZAPI sequence ($A\phi$). The saturation frequency was varied over ±100 kHz in 127 steps. Egg white ZAPISM spectra were acquired from boiled egg white in a 5 mm NMR tube, using a 9.4 T Oxford Instruments magnet interfaced to a Varian Direct Drive console. Saturation RF amplitudes ($\gamma B_1/2\pi$) of 38 and 76 Hz were

used with coherent irradiation ($C\phi$), and peak amplitudes 53 and 107 Hz (rms amplitudes of 38 and 76 Hz) with the ZAPISM sequence ($A\phi$). The saturation frequency was varied over ±30 kHz in 151 steps.

3.1.2. Imaging

In vivo imaging was carried out using a Magnex 4.7 T (Magnex Scientific Ltd., Yarnton, UK) magnet interfaced to a Varian INOVA console (Varian Inc., Walnut Creek, CA, USA) with a volume coil transmit, surface coil receive (Rapid Biomedical GmbH, Rimpar, Germany). Z-spectra were measured using 7 s pre-irradiation and a total time to repetition (TR) of 12 s with saturation RF amplitudes of 30, 100 and 200 Hz. For sinusoidal irradiation the nominal B_1 amplitude was increased by 3 dB to keep the same rms power as in constant amplitude irradiation. The modulation period τ was 200 μs, resulting in $A\phi$ sidebands at ±5 kHz, or ±25 ppm. Images were acquired using a partial fast spin echo (FSE) acquisition (8 echoes/excitation, TE 6 ms, FOV 35×35 mm^2, 1 mm slice, 128×128 pixels), with ZAPISM modulation periods τ of 50, 100, 150, and 200 μs, using a peak RF amplitude of 200 Hz applied on water resonance. As B_1 homogeneity is important in Z-spectroscopy, B_1 maps were measured with a preparation block of 15 flip angles, 45–540°, followed by an FSE readout block as above.

Wistar rats (350–500 g) were anesthetized with i.p. injection of urethane (1.5 g/kg). Breathing frequency was monitored and remained between 100 and 115 min^{-1} in all experiments, with no tendency to change during the study. The core temperature was maintained by a feedback-controlled heating element placed under the animal.

3.2. Data processing

3.2.1. Spectroscopy

The pulse width calibration, T_1 and T_2 calculations, and peak width and integral calculations were carried out using the manufacturer's standard software. All high-resolution spectra were Fourier transformed with 30 Hz line-broadening. The Z-spectral asymmetry $A(\Delta f) = S(f_0 + \Delta f) - S(f_0 - \Delta f)$ was calculated by taking a simple difference between the halves of the Z-spectrum $S(f)$, where f_0 is the water frequency and Δf is the offset from resonance the surrounding frequencies. However, experimental determination of the exact water resonance frequency f_0 is not straightforward. Exact zero frequencies for the experimental Z-spectra were therefore found by fitting the central region to an inverted Lorentzian shape and resampling the Z-spectra at the desired offset frequencies by cubic spline interpolation. In this analysis, the Mathematica 5.2 software package (Wolfram Research Inc., Champaign, IL, USA) was used.

3.2.2. Imaging

Image data were analyzed in Matlab using the Aedes software package (in-house MRI image analysis tool; aedes.uku.fi) and other in-house Matlab routines. As with the spectroscopic data, the conventional Z-spectra were shifted to their exact zero resonances by spline interpolation. In most $A\varphi$ experiments the number of data points was too small for such a procedure, but as the curves following the MT envelope near the points of interest (zero and a few ppm) are virtually flat this was not a problem. As with all other data, images were normalized to a reference scan with saturation offset well beyond the MT range. ROIs in different brain tissue types and muscle were drawn in Aedes. The MT contrast between gray and white matter (GM and WM, respectively) achieved in conventional MT and ZAPISM was characterized by calculating the difference in signals from ROIs drawn in corpus callosum and internal capsule (WM ROI) and in cortex (GM ROI). The differences were compared using a pair-wise *t*-test in which $C\varphi$ at 37.5 ppm was compared to $A\varphi$ at 3 ppm and $C\varphi$ at −37.5 ppm was compared to $A\varphi$ at −3 ppm, for all three RF powers used.

4. Results and discussion

4.1. Phantoms

Z-spectra of boiled egg white obtained at 9.4 T using coherent irradiation ($C\varphi$) and the ZAPI and ZAPISM sequences ($A\varphi$ are shown in Fig. 1 for two rms RF amplitudes. As expected, the constant-phase irradiation results in a conventional Z-spectrum. With alternating-phase ($A\varphi$ irradiation only MT between the short-T_2 protons of the immobilised protein and water contributes to the signal near the water resonance. The amount of MT is dependent on the RF amplitude, as seen in the $C\phi$ experiment. The ZAPI $A\varphi$ experiment displays the expected characteristic pattern of sidebands appearing symmetrically on either side of the water resonance. With ZAPI (blue curve), sidebands appear at $\pm n/\tau$ Hz; when the modulation is changed to sinusoidal (ZAPISM), only the innermost sideband pair is seen (red). Even though the spins at the resonance frequencies of the sidebands experience a lower effective B_1 field than those at the central dip in the $C\varphi$ experiment, giving a narrower line shape, increasing the RF amplitude still broadens the DS pattern of the sidebands, and the inner sidebands contribute slightly to the saturation at the water frequency. This is seen as increased curvature of the $A\phi$ line around the zero frequency for the higher RF amplitude, and may introduce a small non-MT component to the Z-spectral signal at 0 Hz. This can be avoided either by limiting the RF amplitude (narrowing the DS features) or by moving the sidebands further from zero by shortening the modulation period τ. For both approaches there are limiting factors: B_1 must be high enough to produce the desired effects (MT and possibly long T_2 saturation in $C\varphi$ data), and τ must be long enough that the macromolecular pool is saturated effectively. On the other hand, if T_2-selective saturation is of interest, values of τ are naturally shorter, enabling higher RF amplitudes to be used.

Although the MT envelope obtained between sidebands using the $A\phi$ ZAPI sequence follows quite closely the envelope obtained with $C\phi$ irradiation, there are some discrepancies between the two. These may arise because of a distribution of macromolecular T_2s in this phantom, with some components for which the assumption of short T_2 is not completely fulfilled. However, as we will show, in the *in vivo* system studied such discrepancies are negligible. The ZAPISM data, with only two sidebands, follow the $C\varphi$ much more closely.

As discussed earlier, in the analysis of long T_2 features (including those arising from amide protons) the use of the asymmetry of the Z-spectrum can be problematic. In Fig. 2, homogenized rat brain at 9.4 T is used to demonstrate the balance of Z-spectral components near the water resonance. The apparent ME observed between water and aliphatic pools around −5 to −1 ppm on the Z-spectrum is strongly dependent on the RF amplitude used, to the extent that the sign of the asymmetry reverses at the amide resonance as the RF amplitude is increased from 33 Hz to 300 Hz (Fig. 2B). The shape and position of the maximum of the asymmetry curve also change as the irradiation amplitude is varied. The optimum RF amplitude for APTR experiments has been shown to be around 100 Hz [34], as the balance between direct saturation and the amplitude and width of the amide signal is optimal at reasonably low power.

It has been shown previously that at low RF amplitudes, the degree of saturation as a function of pre-irradiation frequency closely parallels the directly-observed spectrum [35]. This suggests the presence either of a non-specific through-space interaction (i.e. a

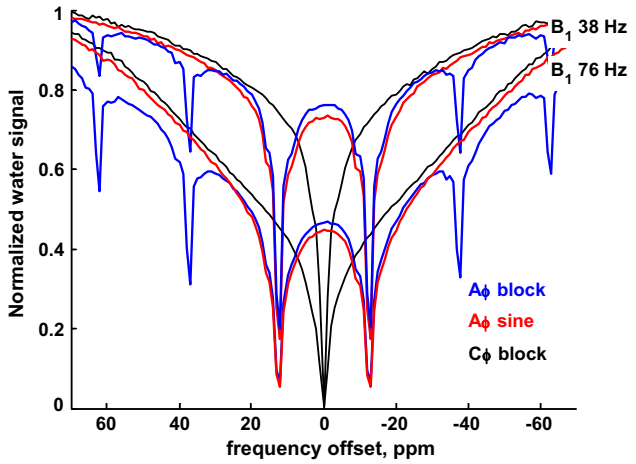

Fig. 1. Z-spectra for constant phase ($C\varphi$, black), alternating phase (ZAPI $A\varphi$, blue) and sine-modulated (ZAPISM $A\varphi$, red) irradiation, for two rms RF amplitudes, measured in heat-denatured egg white at 400 MHz. The number of sidebands is reduced to two with ZAPISM.

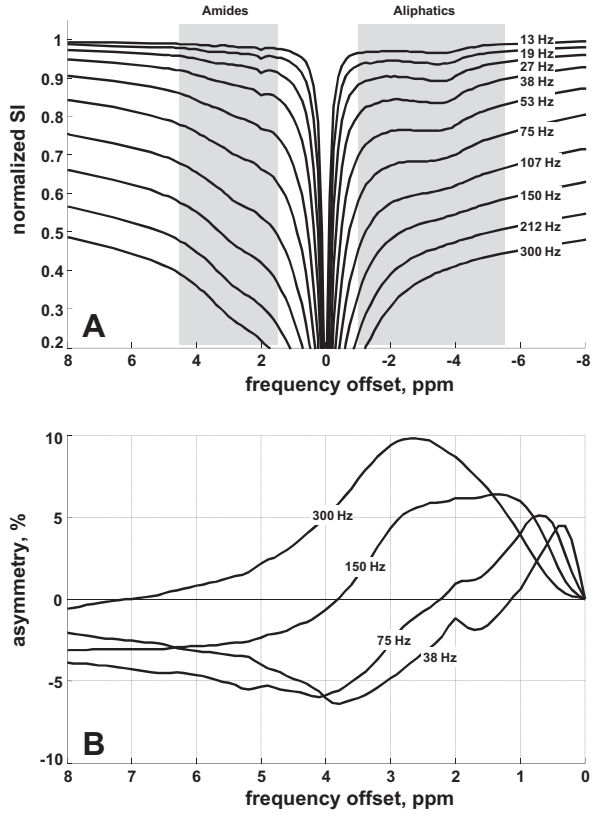

Fig. 2. (A) Normalized Z-spectra of homogenized rat brain at a range of RF amplitudes. (B) Z-spectral asymmetry of homogenized rat brain at a range of RF amplitudes.

direct intermolecular nuclear Overhauser effect, NOE) or, more probably, of chemical exchange tightly coupled to efficient intramolecular spin diffusion. However, at higher RF amplitudes (B_1 = 150 and 300 Hz) there is no apparent intensity drop in the aliphatic region (Fig. 2B). Here the Z-spectrum is dominated by direct saturation of the water resonance and chemical exchange with the amide protons, as shown in numerous other studies [16,18,22,36,37].

4.2. In vivo

The ZAPISM irradiation block was used as a preparation for a fast spin echo MRI sequence. Fig. 3 shows *in vivo* $C\phi$ and $A\phi$ Z-spectra for rat brain cortex and cheek muscle, for $\gamma B_1/2\pi$ = 30, 100, and 200 Hz and a range of offset frequencies. The spectra show the expected dip to zero on resonance in the $C\phi$ images, and only short-T_2 MT attenuation in the ZAPISM $A\varphi$ data. The sidebands in the latter data fall at ±25 ppm (no data points measured, but the structure of the spectrum is similar to those in Fig. 2) and the direct saturation from the sidebands contributes to the $A\varphi$ signal at ±12.5 and ±37.5 ppm when higher irradiation amplitudes (100 and 200 Hz) are used, giving slightly lower signal than on resonance. In brain the two irradiation types coincide very well at ±37.5 ppm, but in muscle tissue MT is greater (partly due to the higher B_1 at the edges of the image) and the $C\phi$ and $A\phi$ intensities differ even at ±37.5 ppm. As previously discussed, this may be due to the presence of some medium-T_2 components in muscle, for which a τ of 200 μs is too short to meet the requirement of incoherent saturation.

As clearly shown in Fig. 2, not only are there additional features in the Z-spectra due to exchange with long-T_2 amide protons, but there is also evidence of interaction between the aliphatic component of the macromolecules and free water at low RF amplitudes. Fig. 4 shows that this is also the case with the brain *in vivo*. The difference between the aliphatic saturation (around −3 ppm from water $C\phi$) and on-resonance MT (ZAPISM $A\phi$), and the amide saturation (around +3 ppm from water $C\phi$) and on-resonance MT (ZAPISM $A\phi$) at a range of B_1 amplitudes is presented. The asymmetry is calculated by subtracting the $C\phi$ images at +3 ppm from the $C\phi$ images at −3 ppm. At the lowest RF amplitude (30 Hz) it is clear that there is also a significant signal from the aliphatic component (negative asymmetry, blue), whereas at the higher RF amplitude, the amide signal is more intense (red). Interestingly, the asymmetry obtained with a B_1 of 100 Hz is stronger than that seen with 200 Hz irradiation. This may be a consequence of the different underlying MT asymmetry, as well as the B_1-dependent line shape of the amide feature in the Z-spectrum. Indeed, as was mentioned previously, the optimal RF amplitude for APT studies has been shown to be around 100 Hz [36]. In conclusion, these results reinforce the message that the use of simple Z-spectral asymmetry to monitor pH-dependent changes in exchange may conceal competing contributions from other sources.

In Fig. 5 the differences between $A\varphi$ and $C\varphi$ data in the MT region (±12.5 and ±37.5 ppm) are shown. In theory, these should result in zero signal but here it is apparent that the direct saturation influences the $C\varphi$ data at 12.5 ppm. The sidebands in $A\varphi$ fall at ±25 ppm, but as they have a narrower DS pattern (lower effective B_1), they have negligible effect. As previously shown, there may also be a contribution from longer-T_2 macromolecular components.

A feature that is not apparent in the *in vitro* samples, but is clear in the *in vivo* data and has been discussed in various other studies [16,22], is the asymmetry of the MT envelope. Fig. 6 shows negative intensity for images of $C\phi$ asymmetry at all offsets, suggesting increased saturation weighted toward the resonance frequencies of the aliphatics. However, in asymmetries calculated from $A\varphi$ data, negative asymmetry is seen at 37.5 ppm while the asymmetry at 12.5 ppm is positive. This may be a result of asymmetry of the macromolecular spectrum at the sidebands at ±25 ppm. Data are shown for a B_1 of 200 Hz, as all saturation amplitudes result in similar behavior.

One key feature of ZAPI is its ability to function as a T_2 filter through appropriate choice of the modulation period τ. In order to saturate the whole macromolecular pool efficiently, τ should be longer than the longest macromolecular T_2; on the other hand,

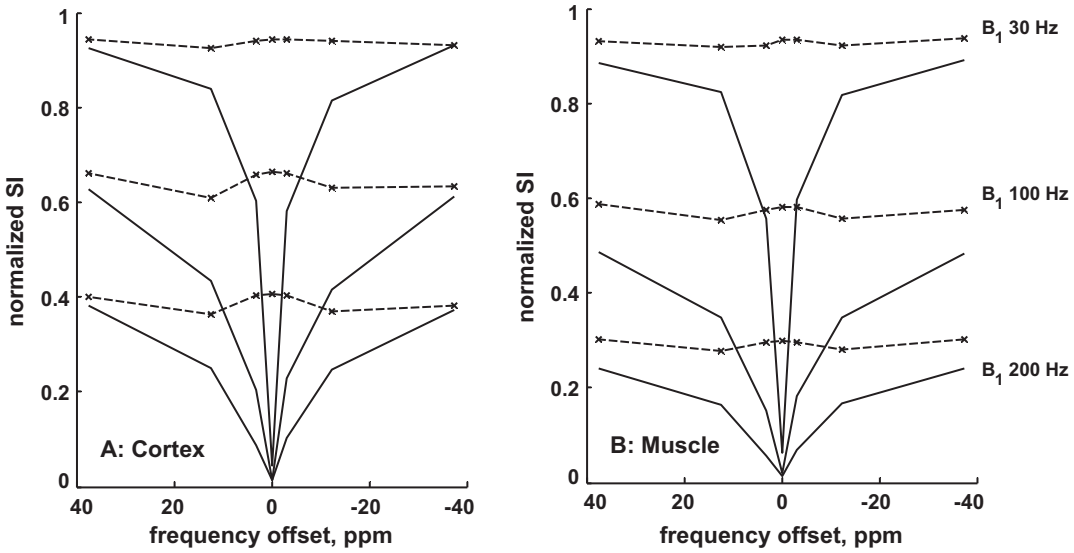

Fig. 3. $C\phi$ (solid lines) and ZAPISM $A\phi$ (dotted lines) data at B_1 equal to 200, 100 and 30 Hz measured from a normal rat head *in vivo* at 4.7 T. Signals from regions of interest located in cortex (A) and cheek muscle (B) are shown.

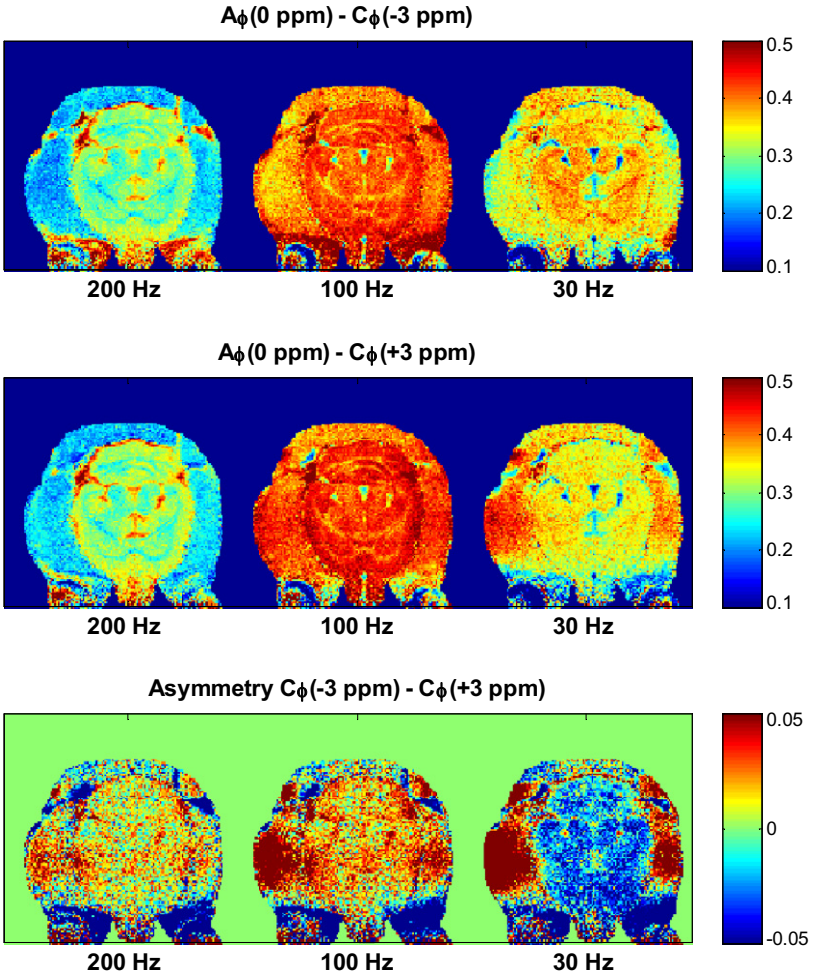

Fig. 4. Images of saturation of long-T_2 components near the water resonance. Top row: difference between the aliphatic $C\phi$ saturation (−3 ppm) and on-resonance MT (0 ppm, $A\phi$). Middle row: subtraction of amide saturation in $C\phi$ (+3 ppm) from on-resonance MT (0 ppm, $A\phi$). Bottom row: ME asymmetry in $C\phi$ at 3 ppm. Note the negative asymmetry with low irradiation amplitude of 30 Hz.

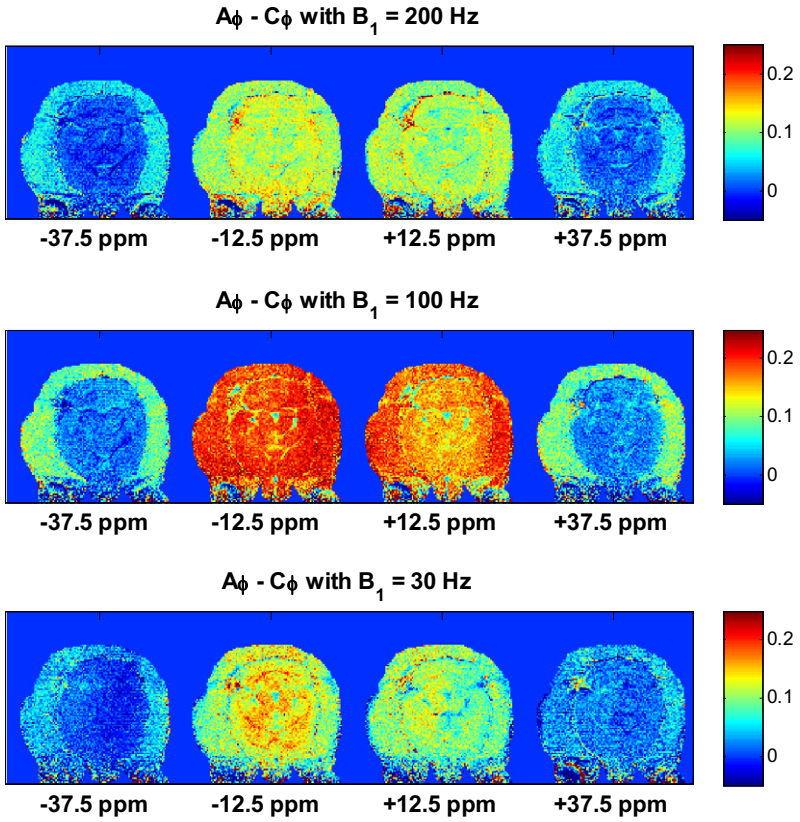

Fig. 5. Differences between ZAPISM and $C\phi$ signal in the conventional MT region far from water resonance in rat head *in vivo*. The sidebands for the ZAPISM experiment fall at ±25 ppm. Differences at ±37.5 ppm are small for the brain tissue, implying that the direct saturation from the sidebands is insignificant. At ±12.5 ppm the ZAPISM signal is higher as the DS from $C\phi$ is stronger than the DS from ZAPISM.

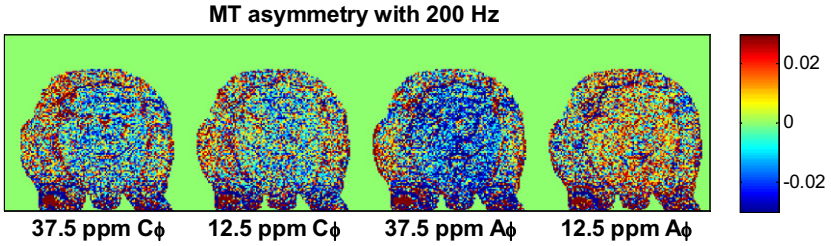

Fig. 6. MT asymmetry: the difference in MT at ±37.5 and ±12.5 ppm offset frequencies for both $C\phi$ and $A\phi$, with B_1 of 200 Hz. The asymmetry is similar in $C\varphi$ and $A\varphi$ at 37.5 ppm but reversed at 12.5 ppm.

τ must be shorter than the T_2 of the components that are to be left unsaturated. In brain and phantoms an appropriate compromise is around 200 μs, corresponding to 5 kHz modulation of the irradiation pulse. The longest T_2 values of the macromolecules which contribute to a MT component in $C\varphi$ are in this range. Using longer τs in the $A\varphi$ experiment does not lead to any additional MT, but the $A\varphi$ experiment still follows the same MT envelope as $C\varphi$ (9.4 T, data not shown). Shortening τ makes the T_2 filter stricter and reduces the degree of saturation, as fewer protons in the macromolecules meet the criterion for saturation. This allows investigation of the macromolecular composition of tissues, as well as changes in macromolecular structure and relaxation properties. When τ is shortened to 20 μs, the MT detected is roughly a quarter of that seen in $C\varphi$. Studying e.g. the ratio between long-τ data and short-τ data can produce a contrast dependent on the distribution of the motional states of macromolecules, potentially providing unique information on tissue status and dynamics.

The variation of MT contrast with τ in rat head is illustrated in Fig. 7, for an RF amplitude of 200 Hz. It is clear that the T_2 filter has different effects for muscle and for brain tissue: changing τ from 200 μs to 50 μs decreases the MT by 50% in muscle while in brain the drop is about 70% (bottom row of Fig. 7; muscle is indicated by white arrow). This suggests that the distribution of proton T_2s involved in MT is weighted more to short components in muscle tissue than in brain. This is consistent with the $C\varphi$ and $A\varphi$ image intensity difference in muscle at ±37.5 ppm, seen in Fig. 3, suggesting a quite different T_2 distribution compared to brain. It should also be noted that the B_1 distribution of the RF coil used here is optimized for the brain region and the B_1 tends to be slightly higher in the peripheral regions, like muscle. This may change the T_2 filtering slightly, as the saturation and MT dynamics are dependent on B_1. Another feature in Fig. 7 is the contrast between grey and white matter; white matter tracts in the cerebellum are highlighted (green arrow). This contrast arises from high myelin

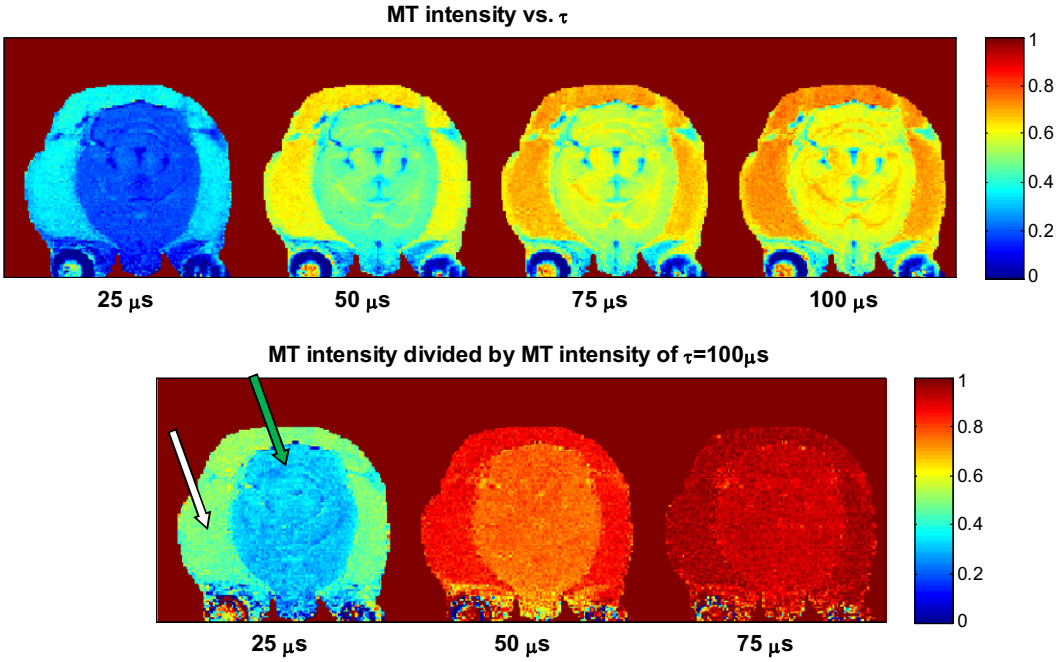

Fig. 7. The effect of modulation period τ on the MT-induced reduction in the water signal. τ is varied from 25 to 100 μs for 200 Hz on-resonance irradiation. The amount of MT is reduced as τ is decreased. The images on the lower row show the ratio of the signal amplitude at a given τ to that for a τ of 200 μs image, illustrating the use of ZAPISM as a macromolecular T_2 filter. A white matter tract in the cerebellum is marked with a green arrow, and muscle tissue with a white arrow.

content increasing the proportion of the macromolecular pool with short T_2. ZAPISM measured at 3 ppm shows significantly better GM/WM contrast than conventional MT at 37.5 ppm ($p = 0.02$ in a pair-wise t-test), which is as expected since ZAPISM exploits the full MT on the zero frequency while methods using an offset saturation operate on the slopes of the MT envelope.

This paper is intended as a proof of principle for the ZAPI technique; experimental demonstration in animal models of diseases, and in the clinical setting, will follow. A well-characterized disease model for the amide exchange balance is ischemic stroke, in which exchange is greatly reduced [38,39]. Similarly, it is well known that the MT, and possibly also the macromolecular T_2 distribution, is altered in diseases affecting the white matter, such as MS disease [40] or traumatic brain injury, in which atrophy of white matter tracts occurs [41].

4.3. Practical aspects of ZAPI implementation

The choice of τ is restricted by the location of the sidebands; this is typically a more severe restriction than T_2-selectivity. Lengthening τ brings the sidebands closer to zero frequency, and therefore DS and/or long T_2 ME components intrude around zero frequency. This may introduce bias both to the on-resonance MT images and to the analysis of, for example, amide peaks. This also restricts the RF amplitudes usable in on-resonance ZAPISM, as the DS feature becomes broader when irradiation power is increased.

If the cycle duration τ is reduced, sidebands move further from the zero resonance and DS becomes less of a problem. Such a reduction is not desirable if the data are to be compared to $C\varphi$ data, as some MT is lost through stricter T_2 filtration, but if the interest is in on-resonance MT itself, a reduced τ enables the use of higher RF amplitudes. MT will be decreased when compared to longer τ experiments, but it can be bought back by increasing B_1 without increasing the DS on resonance.

When the different components of the Z-spectrum need to be separated, both ZAPISM and conventional $C\varphi$ Z-spectra, or points from both, are needed. First, ZAPISM must be run with a loose T_2 filter so that all the macromolecular spins involved in the $C\varphi$ experiment contribute to the MT in ZAPISM. The DS component is the difference between $C\varphi$ and ZAPISM at and near zero offset. If the wings of the DS need to be estimated, DS can be modeled, based on its half-width, as an inverted Lorentzian. ME is the same difference at the ME frequency of interest, if the DS from water is negligible. If not, it has to be estimated and subtracted. The MT envelope can be found from the ZAPISM Z-spectrum outside the sidebands. If needed, the MT signal masked by the sidebands can be determined by repeating the ZAPISM experiment with one or more slower modulation frequencies to fill in the gaps, while maintaining the same MT contribution. In shorter experiments, such as *in vivo* imaging, the number of data points needed is restricted. Even though in theory one point from ZAPISM and one point from a $C\varphi$ irradiation should suffice, finding a suitable τ vs. B_1 vs. T_2-filter window that can give a clean separation at an ME frequency of interest may be challenging, in which case the DS component also needs to be estimated and subtracted.

Any errors in the RF modulation, for example short gaps in the RF envelope because of spectrometer timing limitations, will cause unwanted changes in sideband patterns and artifacts in images. Where instrument hardware has such limitations it can be advantageous to program the irradiation in blocks of multiple phase changes rather than the unit cycle; short timing overhead delays then have negligible effects.

B_1 maps for the imaging setup used typically show variation of 10–20% across the field of view. Within the brain, which is placed at the magnet isocenter and in the middle of the RF coil, the variation is typically 5–10%. The pattern of the variation is itself variable; usually there is a gradient laterally across the brain, but in the experiments shown here the brain region was very homogeneous and the B_1 in the muscle was at worst 15% higher than in brain. Especially when using small B_1 amplitudes, as is the case with ZAPI, the amount of MT is sensitive to the irradiation power. In the comparison of MT between hemispheres, B_1 homogeneity

should be checked, and optimized if a quadrature or multi-channel transmit RF coil is used, as a B_1 gradient alone can cause spurious contrast.

5. Conclusion

Efficient T_2-selective saturation can be achieved by modulation of the saturation pulse using ZAPI. The resulting Z-spectrum closely follows the MT component of a conventional Z-spectrum for a range of saturation amplitudes and samples of different macromolecular structure. The sideband pattern of ZAPI can be simplified by replacing simple phase alternation with sinusoidal modulation (ZAPISM), resulting in a single pair of sidebands at $\pm 1/\tau$ Hz. This is especially desirable in cases where the MT envelope is to be analyzed, either as a source of information or as a component to be eliminated, as most of a ZAPISM Z-spectrum shows pure MT effects.

ZAPI and ZAPISM can be used for *in vivo* MRI to estimate the different contributions from long and short T_2 species, as well as to observe long T_2 components preferentially. The possibility of adjusting the T_2 selection threshold enables macromolecule composition, structure and dynamics to be probed. The method can be used both to create novel contrast in MRI, and as a tool to study the interaction between water and other components in sample systems and in tissue.

Acknowledgments

Financial support from the Sigrid Juselius Foundation (JN), the Academy of Finland (JN) and the Leverhulme Trust (Grant F00120Y to GAM and RAK) is greatly appreciated.

References

[1] S. Forsén, R.A. Hoffmann, Exchange rates by nuclear magnetic multiple resonance. 3. Exchange reactions in systems with several nonequivalent sites, J. Chem. Phys. 40 (1964) 1189–1196.
[2] J. Grad, R.G. Bryant, Nuclear magnetic cross-relaxation spectroscopy, J. Magn. Reson. 90 (1990) 1–8.
[3] S.D. Wolff, R.S. Balaban, Magnetization transfer contrast (MTC) and tissue water proton relaxation in vivo, Magn. Reson. Med. 10 (1989) 135–144.
[4] R.G. Bryant, The dynamics of water-protein interactions, Annu. Rev. Biophys. Biomol. Struct. 25 (1996) 29–53.
[5] R.M. Henkelman, G.J. Stanisz, S.J. Graham, Magnetization transfer in MRI: a review, NMR Biomed. 14 (2001) 57–64.
[6] B.P. Hills, The proton-exchange cross-relaxation model of water relaxation in biolpolymer systems 2. The sol and gel states of gelatin, Annu. Rev. Biophys. Biomol. Struct. 76 (1992) 509–523.
[7] E. Liepinsh, G. Otting, Proton exchange rates from amino acid side chains – Implications for image contrast, Magn. Reson. Med. 35 (1996) 30–42.
[8] G. Otting, NMR studies of water bound to biological molecules, Prog. Nucl. Magn. Reson. Spectrosc. 31 (1997) 259–285.
[9] D.F. Gochberg, R.P. Kennan, M.J. Maryanski, J.C. Gore, The role of specific side groups and pH in magnetization transfer in polymers, J. Magn. Reson. 131 (1998) 191–198.
[10] P.C.M. van Zijl, J. Zhou, N. Mori, J.F. Payen, D. Wilson, S. Mori, Mechanism of magnetization transfer during on-resonance water saturation. A new approach to detect mobile proteins, peptides, and lipids, Magn. Reson. Med. 49 (2003) 440–449.
[11] J.Y. Zhou, J.F. Payen, D.A. Wilson, R.J. Traystman, P.C.M. van Zijl, Using the amide proton signals of intracellular proteins and peptides to detect pH effects in MRI, Nat. Med. 9 (2003) 1085–1090.
[12] R.M. Henkelman, X.M. Huang, Q.S. Xiang, G.J. Stanisz, S.D. Swanson, M.J. Bronskill, Quantitative interpretation of magnetization-transfer, Magn. Reson. Med. 29 (1993) 759–766.
[13] A. Ramani, C. Dlaton, D.H. Miller, P.S. Tofts, G.J. Barker, Precise estimate of fundamental in-vivo MT parameters in human brain in clinically feasible times, Magn. Reson. Imaging 20 (2002) 721–731.
[14] J.G. Sled, G.B. Pike, Quantitative imaging of magnetization transfer exchange and relaxation properties in vivo using MRI, Magn. Reson. Med. 46 (2001) 923–931.
[15] M. Cercignani, G.J. Barker, A comparison between equations describing in vivo MT: the effects of noise and sequence parameters, J. Magn. Reson. 191 (2008) 171–183.
[16] J. Pekar, P. Jezzard, D.A. Roberts, J.S. Leigh, J.A. Frank, A.C. McLaughlin, Perfusion imaging with compensation for asymmetric magnetization transfer effects, Magn. Reson. Med. 35 (1996) 70–79.
[17] C. Morrison, G. Stanisz, R.M. Henkelman, Modeling magnetization-transfer for biological-like systems using a semisolid pool with a super-lorentzian lineshape and dipolar reservoir, J. Magn. Reson. B. 108 (1995) 103–113.
[18] J.Y. Zhou, B. Lal, D.A. Wilson, J. Laterra, P.C.M. van Zijl, Amide proton transfer (APT) contrast for imaging of brain tumors, Magn. Reson. Med. 50 (2003) 1120–1126.
[19] T.L. Hwang, S. Mori, A.J. Shaka, P.C.M. van Zijl, Application of phase-modulated CLEAN chemical EXchange spectroscopy (CLEANEX-PM) to detect water–protein proton exchange and intermolecular NOEs, J. Am. Chem. Soc. 119 (1997) 6203–6204.
[20] J. Zhou, P.C.M. van Zijl, Chemical exchange saturation transfer imaging and spectroscopy, Prog. Nucl. Magn. Reson. Spectrosc. 48 (2006) 109–136.
[21] O.E. Mougin, R.C. Coxon, A. Pitiot, P.A. Gowland, Magnetization transfer phenomenon in the human brain at 7 T, NeuroImage 49 (2010) 272–281.
[22] J. Hua, C.K. Jones, J. Blakeley, S.A. Smith, P.C.M. van Zijl, J. Zhou, Quantitative description of the asymmetry in magnetization transfer effects around the water resonance in the human brain, Magn. Reson. Med. 58 (2007) 786–793.
[23] M. Kim, J. Gillen, B.A. Landman, J. Zhou, P.C. van Zijl, Water saturation shift referencing (WASSR) for chemical exchange saturation transfer (CEST) experiments, Magn. Reson. Med. 61 (2009) 1441–1450.
[24] D.C. Williamson, J. Närväinen, P.L. Hubbard, R.A. Kauppinen, G.A. Morris, Effects of radiation damping on Z-spectra, J. Magn. Reson. 183 (2006) 203–212.
[25] P.K. Madhu, A. Kumar, Bloch equations revisited: new analytical solutions for the generalized Bloch equations, Concepts Magn. Reson. 9 (1997) 1–12.
[26] H.N. Yeung, R.S. Adler, A.G. Swanson, Transient decay of longitudinal magnetization in heterogeneous spin systems under selective saturation. IV. reformulation of the spin-bath-model equations by the Redfield–Provotorov theory, J. Magn. Reson. Ser. A 106 (1994) 37–45.
[27] G.A. Morris, R. Freeman, Selective excitation in Fourier transform nuclear magnetic resonance, J. Magn. Reson. 1978 (1978).
[28] M. Pachot-Clouard, L. Darrasse, Optimization of T_2-selective binomial pulses for magnetization-transfer, Magn. Reson. Med. 34 (1995) 462–469.
[29] J. Forster, F. Schick, M. Pfeffer, O. Lutz, Magnetization-transfer by simple sequences of rectangular pulses, MAGMA 3 (1995) 83–93.
[30] E. Vinogradov, S. Zhang, A. Lubag, J.A. Balschi, A.D. Sherry, R.E. Lenkinski, On-resonance low B1 pulses for imaging of the effects of PARACEST agents, J. Magn. Reson. 176 (2005) 54–63.
[31] N.P. Davies, I.R. Summers, W. Vennart, Optimum setting of binomial pulses for magnetization transfer contrast, J. Magn. Reson. Imaging 11 (2000) 539–548.
[32] S.J. Graham, R.M. Henkelman, Pulsed magnetization transfer imaging: evaluation of technique, Radiology 212 (1999) 903–910.
[33] S.A. Smith, J.A. Farrell, C.K. Jones, D.S. Reich, P.A. Calabresi, P.C. van Zijl, Pulsed magnetization transfer imaging with body coil transmission at 3 Tesla: feasibility and application, Magn. Reson. Med. 56 (2006) 866–875.
[34] P.Z. Sun, P.C.M. van Zijl, J.Y. Zhou, Optimization of the irradiation power in chemical exchange dependent saturation transfer experiments, J. Magn. Reson. 175 (2005) 193–200.
[35] P.L. Hubbard, J. Närväinen, R.A. Kauppinen, G.A. Morris, Unexpected magnetization transfer to aliphatic resonances in Z-spectroscopy in model systems, in: Proc. ISMRM 16th Ann. Meeting, Berlin, Germany, 2006, p. 3464.
[36] A.D. Stein, D.A. Roberts, J. McGowan, R. Reddy, J.S. Leigh, Asymmetric cancellation of magnetization transfer effects, in: 2nd Ann. Meeting of SMR, San Francisco, CA, USA, 1994, p. 880.
[37] S.D. Swanson, Y. Pang, MT is symmetric but shifted with respect to water, in: Proc. ISMRM 11th Ann. Meeting, Toronto, Canada, 2003, p. 660.
[38] K.T. Jokivarsi, H.I. Grohn, O.H. Grohn, R.A. Kauppinen, Proton transfer ratio, lactate, and intracellular pH in acute cerebral ischemia, Magn. Reson. Med. 57 (2007) 647–653.
[39] P.Z. Sun, J. Zhou, W. Sun, J. Huang, P.C. van Zijl, Detection of the ischemic penumbra using pH-weighted MRI, J. Cereb. Blood Flow Metab. 27 (2007) 1129–1136.
[40] M. Cercignani, G. Iannucci, M.A. Rocca, G. Comi, M.A. Horsfield, M. Filippi, Pathologic damage in MS assessed by diffusion-weighted and magnetization transfer MRI, Neurology 54 (2000) 1139–1144.
[41] A.E. Mamere, L.A. Saraiva, A.L. Matos, A.A. Carneiro, A.C. Santos, Evaluation of delayed neuronal and axonal damage secondary to moderate and severe traumatic brain injury using quantitative MR imaging techniques, Am. J. Neuroradiol. 30 (2009) 947–952.